

# Origin and geochemical evolution from ferrallitized clays to karst bauxite: An example from the Lower Cretaceous of NE Spain



Alfonso Yuste\*, Blanca Bauluz, María José Mayayo

IUCA-Grupo Recursos Minerales, Departamento de Ciencias de la Tierra, Universidad de Zaragoza, Pedro Cerbuna 12, 50009 Zaragoza, Spain.

## ARTICLE INFO

### Article history:

Received 21 October 2016  
Received in revised form 19 December 2016  
Accepted 30 December 2016  
Available online 31 December 2016

### Keywords:

Karst bauxite  
Ferrallitization  
Lower Cretaceous  
Weathering  
Geochemistry  
REE

## ABSTRACT

Four outcrops of Lower Cretaceous (Barremian) karst bauxites located in Teruel (NE Spain) were analysed. The deposits show a heterogeneous-chaotic lithostructure consisting of pisolitic bauxite blocks embedded in lateritic red clays filling karst cavities. The research has focused on the geochemical study of major, minor, and trace elements (including some critical to industry) of both the bauxites and clays. The objective was to investigate the bauxite precursor material and to characterize the system's geochemical evolution. Geochemical analyses were carried out by inductively-coupled plasma optical emission and mass spectroscopy. An absolute weathering index has been calculated to estimate element mobility, assuming Ti as an immobile element and the Upper Continental Crust (UCC) as parent material. Further, selected samples were observed by field emission scanning electron microscopy. The data indicate that both the bauxites and red clays originated by intense chemical weathering from more mafic argillaceous sediments than the UCC. Ongoing weathering caused the bauxitization of the upper parts of the original profile, preventing the lower parts from being bauxitized, thus producing the ferrallitized clays underlying the pisolitic bauxites. Subsequent karst reactivation gave rise to the current lithostructure. Ferrallitization is related to Fe, Sc, and V enrichment. On the other hand, although bauxites are relatively enriched in some elements compared to clays, the more intense chemical weathering associated with bauxitization led to chemical homogenization and widespread element depletion. During the bauxitization, Al, Ti, Zr, Cr, and probably Hf and the critical element Nb behaved as more immobile elements in the system. Bauxitization also enhanced homogenization and depletion of the REE, which is more pronounced for the LREE. HREE trends seem to be partly related to the concentration of Ti oxides in the bauxites, whereas P-bearing phases, more frequent in the clays, control the LREE. Subsequent to bauxitization, partial kaolinization of the bauxite took place related to the circulation of acid solutions that also caused the karst reactivation. These late processes caused some Al depletion in the bauxites and enhanced Fe loss together with V and, to a lesser extent, Ge.

© 2017 Elsevier B.V. All rights reserved.

## 1. Introduction

Bauxitization is a special case of chemical weathering (Bardossy, 1982). Chemical weathering is a major mechanism that partitions elements between crustal rocks and natural water (Taylor and McLennan, 1985); it is completely dependent on the (climate-driven) water cycle (Tardy, 1986). During chemical weathering, the differentiation of elements depends on element mobility, and the degree of chemical differentiation depends on the intensity of chemical weathering. Accordingly, major, minor, and trace elements are fractionated during bauxitization, and therefore the distribution of mobile elements can reflect the inten-

sity of weathering and the distribution of immobile elements can be used to identify precursor rocks. Molecular proportions of  $Al_2O_3$ , CaO,  $Na_2O$ , and  $K_2O$  are used to calculate the Chemical Index of Alteration (CIA) (Nesbitt and Young, 1982), which has been utilized in a number of studies to determine the degree of weathering. In bauxite formation, many studies have recognized Al as an immobile element (e.g. Sastri and Sastry, 1982; Valeton et al., 1987; Gow and Lozej, 1993), and high correlations between Al and some major and trace element contents indicate immobile element pairs during the bauxitization process (MacLean, 1990). Most of the geochemical research has also evidenced the relatively immobile behaviour of a group of trace elements (e.g. Sc, Co, Cr, and Zr) in the surficial environment. Furthermore, REE abundance varies in weathering products and is accepted as a marker of their source rocks (e.g. Schellmann, 1986; Taylor and McLennan, 1995;

\* Corresponding author.

E-mail address: [alfon@unizar.es](mailto:alfon@unizar.es) (A. Yuste).

Nyakairu and Koeberl, 2001). What is more, Eu anomalies and  $(La/Yb)_N$  ratios depend on fractionation during bauxitization (Cullers and Graf, 1983; Maksimovic and Pantó, 1991; Mongelli, 1997; Mameli et al., 2007). In consequence, a number of studies have shown that immobile elements are a powerful tool to decipher the genetic history of karst bauxite deposits (e.g. Maksimovic and Pantó, 1991; MacLean et al., 1997; Mongelli, 1997; Mameli et al., 2007; Liu et al., 2013).

According to Bardossy (1982), bauxite deposits overlying carbonate rocks are called karst bauxite deposits regardless of whether the bedrock surface is karstified or not, or of the degree of karstification (Mameli et al., 2007). Among karst bauxites, a great majority are Mediterranean-type, which frequently shows moderately to strongly karstified bedrock surfaces (Bardossy, 1982). Karst bauxite deposits from NE Spain are of this type and occur in three main zones: the South Pyrenean Zone, Catalanian Coastal Range, and Maestrazgo. Our study focuses on one of the most representative deposits located in the Maestrazgo zone, the Lower Cretaceous (Barremian) Fuentespalda deposit (Teruel, NE Spain) (Molina and Salas, 1993). Previous studies based on mineralogical and textural features of the Fuentespalda deposit have proposed a complex sequence of processes to explain the bauxite genesis, mainly through the transformation of precursor lateritic clays into pisolitic bauxites (Yuste et al., 2015). According to these authors, bauxitization occurred as a result of intense chemical weathering under seasonal subtropical climate conditions that favoured several pulses during the bauxitization process.

Although the Maestrazgo bauxite deposits no longer have any economic value, understanding the genetic processes and geochemical evolution that led to their formation is a valuable means to decipher the behaviour of chemical elements during bauxitization. This can be of special interest in the case of those elements critical to industry, such as REE, Nb, Ga, and Ge, listed in the 2014 European Union report on critical raw materials and usually found in karst bauxites (Mongelli et al., 2014). In consequence, as Mongelli et al. (2016) summarizes, recent research has dealt with the processes that control the distribution of economic elements in karst bauxite deposits.

Our research focuses on the geochemical study of major, minor, and trace elements of the Fuentespalda karst bauxite deposit (NE Spain), which is a good example of bauxite closely related to lateritic clay materials. Our goal was to investigate the precursor material of the bauxites and to characterize the geochemical evolution of the bauxitization process.

## 2. Geological framework

The bauxite deposit studied is Early Cretaceous (Barremian) in age and located in the Maestrazgo zone (Fig. 1), which is one of the three most important bauxite regions in NE Spain. During the Mesozoic, the spread of the Tethys westwards and the opening of the North Atlantic Ocean led to the development of a rift system in Iberia. The Iberian rift remained active until the Mid Cretaceous and controlled the late Palaeozoic and the Mesozoic sedimentation

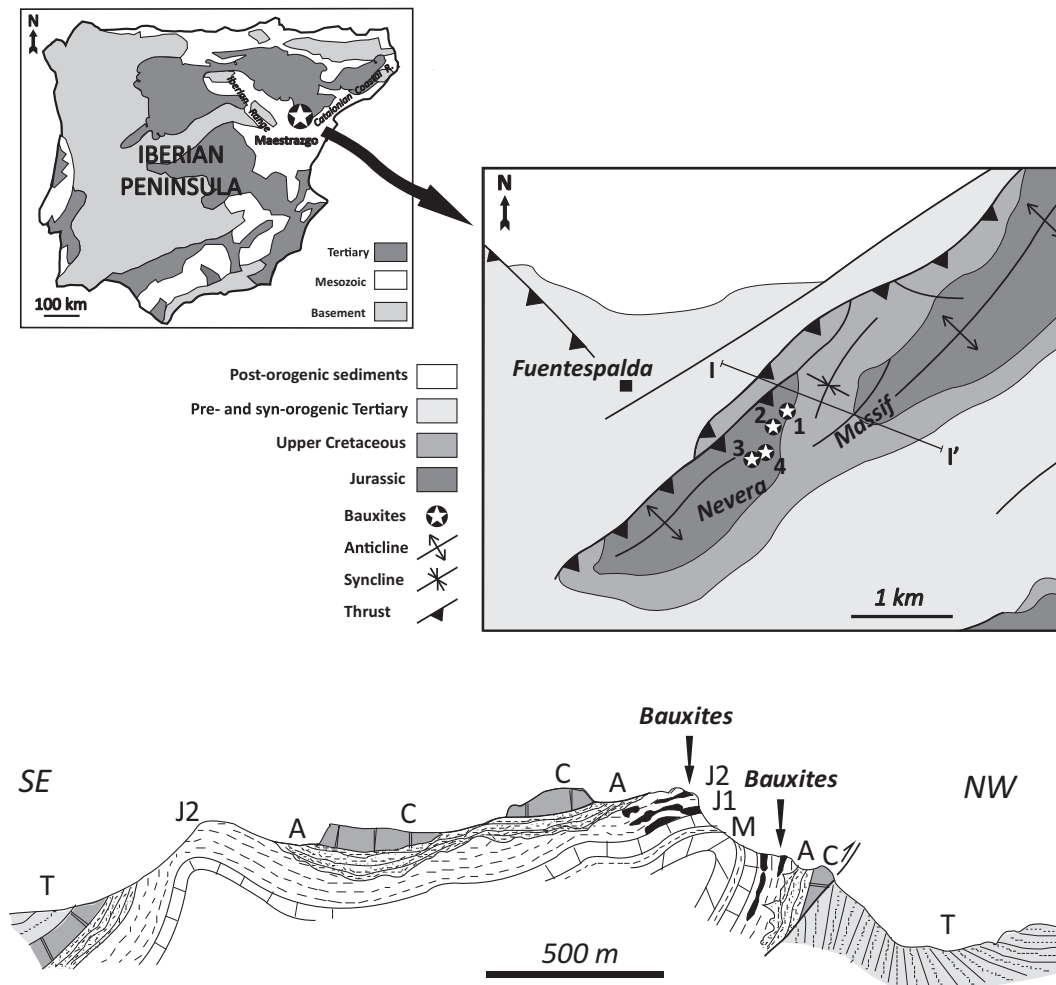


**Fig. 1.** Geological framework of the study area located in the Maestrazgo zone (NE Spain) and geological sketch of the location of the study outcrops (stars). I-I' on the map corresponds to the cross-section below. M: Middle Jurassic, J1: Oxfordian, J2: Polpis Fm., A: Arenas de Utrillas Fm., C: Cenomanian, T: Tertiary.

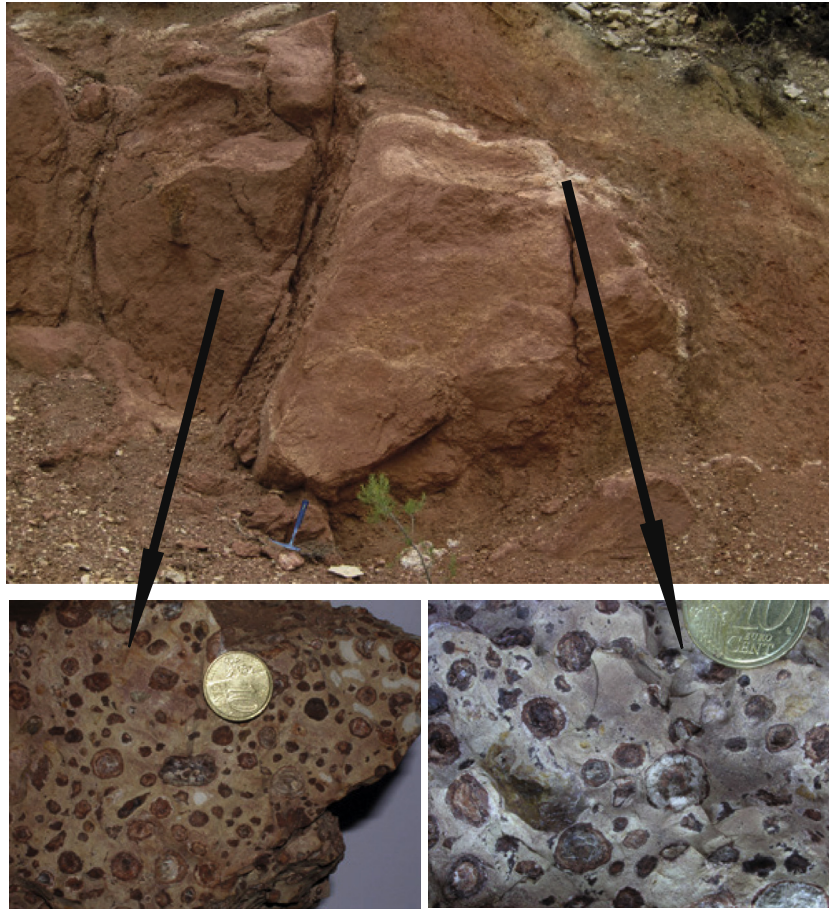


**Fig. 2.** Field appearance of the heterogeneous-chaotic lithostructure of the study materials in one of the outcrops (locality 2 in Fig. 1) and hand specimens of red (left) and white (right) pisolitic bauxites. Scale: coin is 2 cm in diameter. (For interpretation of the references to colour in this figure legend, the reader is referred to the web version of this article.)

in the study area. One of the most active stages of this rifting process took place during the Late Jurassic–Early Cretaceous (Salas and Casas, 1993; Van Wees et al., 1998) and was responsible for the creation of several basins with high subsidence rates (Mas et al., 1998; Salas et al., 2001; Mas and Salas, 2002). The first of these basins was the Maestrazgo Basin (Guimerà et al., 2004), where a clear predominance of marine carbonates and marls characterized sedimentation during the Late Jurassic (Mas et al., 2004). As the rifting stage progressed, tectonic activity was attenuated and subsidence rates decreased during the Early Cretaceous (Valanginian–Barremian) (Mas et al., 2004). The sedimentary record during this time in the Maestrazgo Basin was controlled by very shallow carbonate platforms subject to significant continental influence, giving rise to large lacustrine-palustrine areas (Mas et al., 2004).

The study area shows considerable development of folds and thrusts affecting the Mesozoic formations, with predominant E–W strike orientations. These structures are conditioned upon basement faults that also controlled the main palaeogeographic characteristics during Mesozoic sedimentation (Molina and Salas, 1993). These features constrain the current location of the study deposits, which crop out in a NW-verging anticlinal thrust affecting Jurassic and Cretaceous rocks surrounded by continental Cenozoic materials (Molina and Salas, 1993) (Fig. 1).

The bauxite and related clay materials constitute bodies filling karst cavities developed in limestones and argillaceous limestones of Upper Oxfordian–Kimmeridgian age, constituting the Polpis Formation (Salas, 1987). Some bodies are lens-shaped and concordant

with the stratification of the host rocks. Nevertheless, the original morphology of the cavities, exposed by small quarries and trenches from past mining activity, is frequently modified by brecciation associated with radial acicular calcite cements (Molina and Salas, 1993). Materials filling the cavities have a heterogeneous-chaotic lithostructure (Bardossy, 1982) consisting of up to meter-sized pisolitic bauxite blocks, sometimes fractured or faulted, embedded in red clays (Fig. 2). Pisolitic bauxites are mainly red, but predominantly white zones are also frequently observed in the upper parts of blocks (Fig. 2). The paleokarst is fossilized by the Arenas de Utrillas Formation (Albian) and/or by Cenomanian dolomitized limestones (Molina and Salas, 1993). Important outcrops of ferrallitized clays exist in the vicinity of the studied karstic bauxites (Combes, 1969). Lateritic clays from the Barremian Cantaperdius Formation (Salas, 1987) crop out in the proximity of the study area (approximately 10–15 km southeast of Fuentespalda) near the localities of Beceite (Teruel) and Fredes (Castellón). These lateritic clays also commonly overlie karstified carbonate strata, show a similar composition to the clay materials related to the studied bauxite and displaying frequent pisolitic levels indicating, as Molina and Salas (1993) pointed out, that they are laterally related to the bauxites and associated clays from Fuentespalda.

### 3. Methods

Samples were taken from four outcrops (localities 1–4 in Fig. 1). A set of fourteen samples from the pisolitic bauxite (nine samples) and the red clays (five samples) constituting the infill material of

the karst cavities have been analysed. Pisolitic bauxite samples have been divided into red pisolitic and white pisolitic. Further, one host limestone sample and one sample of the observed acicular radial calcite cements have also been analysed. The first number of sample labels in the data tables indicates the locality number.

Chemical analyses of major and trace elements of bulk samples were performed at Actlabs Laboratories (Canada) using the following techniques (detection limits in brackets): major elements (0.01%, except MnO and TiO<sub>2</sub> with detection limits of 0.001%) and trace elements V (5 ppm), Sr (2), Ba (3), Sc (1), and Be (1) by inductively coupled plasma/optical emission spectroscopy (ICP/OES). The other trace elements, such as Cr (20 ppm), Co (1), Ni (20), Rb (1), Cs (0.1), Th (0.05), U (0.01), Y (0.5), Zr (1), Nb (0.2), Hf (0.1), La (0.05), Ce (0.05), Pr (0.01), Nd (0.05), Sm (0.01), Eu (0.005), Gd (0.01), Tb (0.01), Dy (0.01), Ho (0.01), Er (0.01), Tm (0.005), Yb (0.01), and Lu (0.002) were determined by inductively coupled plasma/mass spectroscopy (ICP/MS). Fused samples (lithium metaborate/tetraborate fusion) were run for major oxides and V, Sr, Ba, Sc, and Be on a combination simultaneous/sequential Thermo Jarrell-Ash ENVIRO II ICP or a Varian Vista 735 ICP. Calibration is performed using seven prepared USGS and CANMET certified reference materials. One of the seven standards is used during the analysis for every group of ten samples. For the analysis of the other trace elements, fused samples are diluted and analysed by Perkin Elmer Sciex ELAN 6000, 6100 or 9000 ICP/MS. Three blanks and five controls are analysed per group of samples. Duplicates are fused and analysed every 15 samples.

Selected samples (11) were analysed by field emission SEM (FESEM) using backscattered electron (BSE) and energy-dispersive X-ray (EDS) analyses. The observations were performed using a JEOL JSM 6400 (SEM) equipped with an Oxford instrument detector (EDS) and a Carl Zeiss MERLIN FESEM. The accelerating voltage was 4–15 kV with a beam current of 1–2 nA and a counting time of 50 s. Samples were carbon coated.

An absolute weathering index (Nesbitt, 1979) has been calculated to estimate element mobility, assuming Ti as an immobile element and the Upper Continental Crust (UCC; Taylor and McLennan, 1985) as parent material. According to Nesbitt (1979), the percentage increase or decrease (change %) on any element X compared with its concentration in the parent material is given by  $[(X_{\text{sample}}/Ti_{\text{sample}})/(X_{\text{UCC}}/Ti_{\text{UCC}}) - 1] * 100$ . The Chemical Index of Alteration (CIA; Nesbitt and Young, 1982) has been calculated using molecular proportions of the following oxides:  $CIA = (Al_2O_3/Al_2O_3 + CaO^* + Na_2O + K_2O) * 100$ , where CaO\* represents the amount of CaO associated with the silicate fraction of the rock.

## 4. Results

The mineralogical analysis by X-ray Diffraction was the subject of a previous paper (Yuste et al., 2015). Despite this, we include here a brief summary essential to properly discussing and interpreting the geochemical study carried out in the current research. The average mineralogical composition of the samples is shown in Table 1. In whole sample, pisolitic bauxites show kaolinite (Kln),

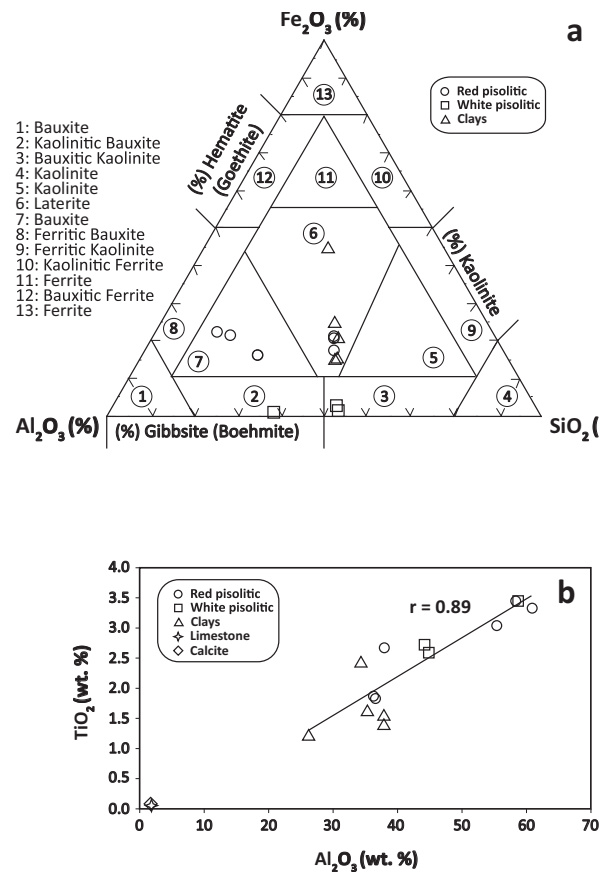


Fig. 3. a: Plot of Al<sub>2</sub>O<sub>3</sub> vs. TiO<sub>2</sub>. b: Fe<sub>2</sub>O<sub>3</sub>-SiO<sub>2</sub>-Al<sub>2</sub>O<sub>3</sub> diagram after Aleva (1994) of bauxite chemical classification.

**Table 1**  
Mineralogical composition (%) of the study samples (min.: minimum; max.: maximum; st. dv.: standard deviation). Kln: kaolinite; Gbs: gibbsite; Gt: goethite; Hem: hematite, Dsp: diaspore; Bhm: boehmite; Ant: anatase; Rt: rutile; Ill: illite; Qtz: quartz; Cal: calcite; tr: traces.

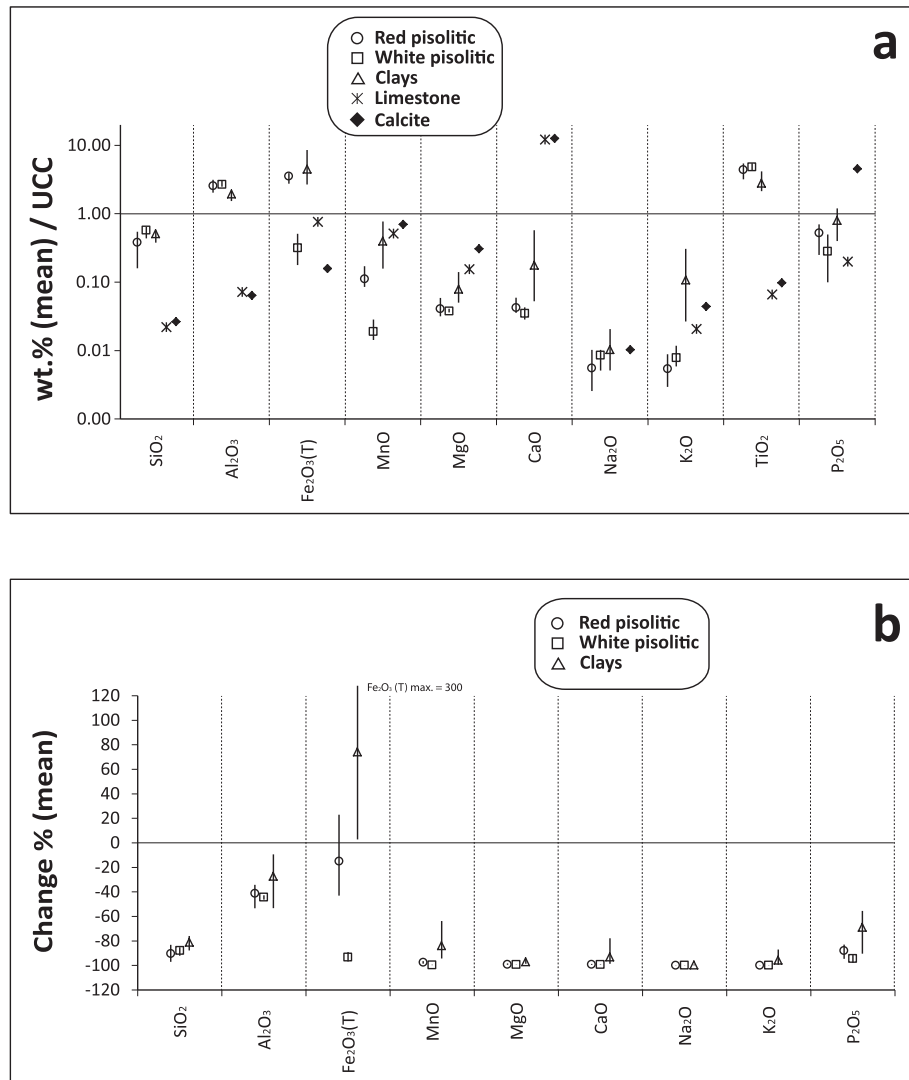
Sample description		Whole sample										<2 μm fraction		
		Kln	Gbs	Gt	Hem	Dsp	Bhm	Ant	Rt	Ill	Qtz	Cal	Ill	Kln
Red pisolitic (n = 6)	mean	55	22	3	10	6	tr.	tr.	tr.	–	tr.	–	tr.	100
	min.	28	0	0	8	5								100
	max.	83	45	7	12	8								100
	st. dv.	22	22	3	1	1								0
White pisolitic (n = 3)	mean	78	10	2	–	6	tr.	tr.	tr.	–	–	–	tr.	100
	min.	57	0	0		5								100
	max.	92	31	5		7								100
	st. dv.	15	15	2		1								0
Clays (n = 5)	mean	66	–	12	7	4	–	tr.	tr.	4	tr.	1	11	89
	min.	44		0	0	0				0		0	0	60
	max.	79		25	18	9				18		5	40	100
	st. dv.	13		9	7	4				7		2	16	16

**Table 2**  
Chemical composition of the analysed samples. Major elements in weight per cent (wt%) and trace elements in parts per million. wt% oxides recalculated to 100% on a volatile-free basis.

		Sample	SiO <sub>2</sub>	Al <sub>2</sub> O <sub>3</sub>	Fe <sub>2</sub> O <sub>3</sub> (T)	TiO <sub>2</sub>	MnO	MgO	CaO	Na <sub>2</sub> O	K <sub>2</sub> O	P <sub>2</sub> O <sub>5</sub>	S	Sc	V	Cr	Co	Ni	Cu	Rb	Sr	Y	Zr	Nb	Cs	Ba	Hf
Red pisolitic	F1-2	41.09	36.61	20.03	1.83	0.01	0.08	0.21	0.03	0.01	0.09	0.01	38	403	230	8	50	10	<1	101	36.3	345	27.6	0.4	13	9.2	
	F1-3	40.65	36.26	20.66	1.87	0.01	0.15	0.19	0.05	0.04	0.13	0.01	22	475	200	5	50	10	<1	69	34	349	28.8	0.3	13	9.3	
	F2-3	13.48	60.88	21.56	3.33	0.01	0.13	0.32	0.01	0.04	0.17	0.08	39	476	350	3	60	10	<1	39	56.7	610	52.1	0.4	14	15.6	
	F2-4	42.12	37.94	16.88	2.67	0.01	0.08	0.20	0.02	0.01	0.06	0.00	28	381	200	5	80	20	<1	134	48.1	513	47.1	0.1	6	13.5	
	F3-1R	25.50	55.37	15.57	3.04	0.01	0.10	0.19	0.01	0.03	0.15	0.04	33	443	360	5	80	90	<1	312	44.7	554	49.1	0.4	11	14.6	
	F4-2	16.94	58.53	20.53	3.45	0.01	0.11	0.20	0.03	0.01	0.18	0.02	36	480	320	8	40	<10	<1	79	53	627	50.1	0.5	14	16.5	
White pisolitic	F2-2	49.89	44.25	2.70	2.72	0.00	0.11	0.21	0.05	0.05	0.02	0.01	24	165	260	5	70	20	<1	63	43.9	517	46.6	0.4	12	13.6	
	F2-6	50.70	44.89	1.42	2.58	0.00	0.10	0.17	0.05	0.02	0.06	0.01	18	210	270	7	110	30	<1	268	42.2	477	43.9	0.4	9	12.4	
	F3-1B	36.38	58.72	1.01	3.46	0.00	0.10	0.15	0.03	0.03	0.13	0.01	30	183	310	9	100	140	<1	258	48.5	604	52.4	0.3	11	15.9	
Clays	F1-1	43.02	37.91	14.11	1.53	0.02	0.14	2.83	0.04	0.24	0.15	0.02	24	297	190	12	80	20	12	251	35.6	278	21.2	2.1	48	7.7	
	F2-1	28.08	26.34	43.24	1.20	0.06	0.12	0.58	0.03	0.14	0.16	0.04	39	452	190	23	100	50	6	73	41.5	225	20.3	1.1	24	5.7	
	F2-5	38.91	34.33	23.66	2.42	0.03	0.14	0.29	0.02	0.10	0.09	0.01	33	420	240	11	100	30	5	100	54.1	468	41.7	1	23	12.2	
	F1-4	41.27	35.35	20.18	1.61	0.01	0.36	0.36	0.05	0.44	0.28	0.09	22	337	190	26	110	80	22	99	85.1	286	22.9	4.5	71	7.8	
	F3-2	43.80	37.88	14.83	1.38	0.04	0.25	0.26	0.09	1.21	0.25	0.01	47	269	200	35	120	100	52	300	128	234	24.9	6.3	203	6.1	
Limestone	2.52	1.90	5.97	0.06	0.06	0.59	88.68	0.00	0.12	0.07	0.03	12	36	40	<1	<20	10	4	75	28.9	10	1.1	0.9	11	0.2		
Calcite	2.99	1.66	1.22	0.08	0.08	1.17	90.37	0.07	0.26	1.56	0.54	3	24	20	<1	<20	<10	7	45	32.7	10	<0.2	1.3	12	0.3		
cement																											

		Sample	Th	U	La	Ce	Pr	Nd	Sm	Eu	Gd	Tb	Dy	Ho	Er	Tm	Yb	Lu	CIA	∑REE	∑LREE	∑HREE	Eu/Eu*	Ce/Ce*	(La/Sm)c	(Gd/Yb)c	(La/Yb)c
Red pisolitic	F1-2	30.7	3.92	7.53	35.4	2.01	9.91	3.39	0.837	4.86	1	6.5	1.41	4.38	0.721	5.31	0.888	99.81	84.15	58.24	25.07	0.63	2.02	1.40	0.74	0.96	
	F1-3	27.8	3.95	15.7	29.3	2.9	11.1	2.79	0.615	3.52	0.75	4.78	1.09	3.54	0.582	3.94	0.635	99.68	81.24	61.79	18.84	0.60	0.91	3.54	0.72	2.69	
	F2-3	45.2	23.5	14.5	30	2.34	10.3	3.67	0.951	5.67	1.26	8.83	1.88	5.75	0.919	6.27	0.996	99.90	93.34	60.81	31.58	0.64	1.01	2.49	0.73	1.56	
	F2-4	29.8	6.92	22.3	55.4	4.5	18.5	4.38	0.972	5.11	1.09	7.44	1.61	4.97	0.804	5.41	0.84	99.87	133.33	105.08	27.27	0.63	1.18	3.20	0.77	2.79	
	F3-1R	39.9	13.7	25.5	37.3	3.89	12.4	2.89	0.742	4.25	0.95	6.93	1.52	4.69	0.746	5.11	0.825	99.91	107.74	81.98	25.02	0.65	0.75	5.55	0.67	3.37	
	F4-2	43.3	14.2	8.19	23.5	2.35	9.96	3.28	0.852	5.1	1.23	8.4	1.85	5.77	0.931	6.45	1.03	99.91	78.89	47.28	30.76	0.64	1.26	1.57	0.64	0.86	
White pisolitic	F2-2	33.8	6.38	16.9	54.1	3.49	12.7	2.83	0.651	3.74	0.87	6.39	1.49	4.65	0.764	5.24	0.859	99.71	114.67	90.02	24.00	0.61	1.54	3.76	0.58	2.18	
	F2-6	34.3	6.2	36.2	62.1	7.14	29.7	5.01	0.999	4.78	0.97	6.48	1.39	4.27	0.666	4.58	0.726	99.77	165.01	140.15	23.86	0.62	0.81	4.55	0.85	5.34	
	F3-1B	43.7	20.9	18.5	32.6	3.44	12.4	2.89	0.72	4.39	1.02	7.54	1.61	5.09	0.838	5.9	0.971	99.88	97.91	69.83	27.36	0.62	0.86	4.03	0.60	2.12	
Clays	F1-1	22.5	3.2	52.5	93.3	9.69	35.9	7.72	1.39	5.36	0.9	5.24	1.13	3.54	0.563	3.95	0.637	99.18	221.82	199.11	21.32	0.66	0.87	4.28	1.10	8.98	
	F2-1	20.2	9.61	40.9	77.6	7.35	27.6	5.95	1.22	5.71	1.02	6.2	1.27	3.78	0.572	3.8	0.59	99.24	183.56	159.4	22.94	0.64	0.93	4.33	1.22	7.27	
	F2-5	30.9	8.69	46.4	88.2	7.39	26	5.11	1.14	5.7	1.23	8.2	1.76	5.48	0.887	6.02	0.949	99.56	204.47	173.1	30.23	0.65	0.96	5.72	0.77	5.21	
	F1-4	17.1	5.29	98.1	133	13.5	45.9	8.86	1.91	9.15	1.58	9.66	2.05	6.22	0.932	6.03	0.973	98.47	337.87	299.36	36.60	0.65	0.70	6.97	1.23	10.99	
	F3-2	24.6	10	259	285	44.8	144	19.7	3.51	14.9	2.66	16.4	3.39	10.1	1.47	9.41	1.41	96.27	815.75	752.5	59.74	0.63	0.55	8.28	1.28	18.60	
Limestone	1.08	1.74	12.5	12.7	3.2	16.9	4.35	0.947	4.3	0.65	3.29	0.63	1.66	0.229	1.35	0.194	-	62.90	49.65	12.30	0.67	0.43	1.81	2.58	6.26		
Calcite	1.04	6.03	23.1	13.5	4.16	18.2	3.74	0.795	4.02	0.61	3.21	0.65	1.85	0.233	1.23	0.168	-	75.47	62.7	11.97	0.63	0.28	3.89	2.65	12.69		
cement																											



**Fig. 4.** a: Average and range values of major element concentrations normalized to the Upper Continental Crust (UCC) concentrations (Taylor and McLennan, 1985). b: Average and range of major elements change % values.

gibbsite (Gbs), diaspore (Dsp), goethite (Gt), and hematite (Hem), accompanied by traces of boehmite (Bhm), anatase (Ant), rutile (Rt), and occasionally quartz (Qtz). The clayey samples are composed of kaolinite, goethite, hematite, diaspore, and illite or muscovite, along with accessory anatase, rutile, quartz, and calcite (Cal). Kaolinite is very abundant in both the pisolitic and the clay samples, whereas gibbsite, always accompanied by boehmite, is only present in some pisolitic samples, both white and red. The other common Al hydroxide in bauxites, diaspore, has been identified in all the samples. Clays and red pisolitic samples always contain hematite and frequent goethite, whereas these minerals are generally absent in the white pisolitic samples. Rutile and, to a greater extent, anatase have been identified in all the samples. In the <2  $\mu\text{m}$  fraction, kaolinite is the major and almost the only phyllosilicate except in the clays, where illite is always detected and can reach up to 40%. Kaolinites from the clay samples are less ordered and less crystalline than those from the pisolitic samples. Among the pisolitic samples, kaolinites from the white ones are the most crystalline.

In the  $\text{Fe}_2\text{O}_3\text{-Al}_2\text{O}_3\text{-SiO}_2$  classification diagram by Aleva (1994) (Fig. 3a), the clays are classified as laterites, whereas the red pisolitic samples fall in both the laterite and the bauxite fields and the

white pisolitic in the kaolinitic bauxite and bauxitic kaolinite fields. The samples falling in the bauxite and kaolinitic bauxite fields are those containing gibbsite and boehmite.

Si, Al, Fe, and Ti concentrations on average account for 99.04% of the major elements (Table 2) except in the host limestone and the calcite cement sample, where Ca is the most abundant element. In general, major element concentrations reflect the mineralogical composition, with the highest Al contents in samples with gibbsite and boehmite and low Fe contents in white pisolitic samples (scarce or absent Fe oxides). Mg is mainly related to illite, as suggested by its higher concentrations in the clays. Nevertheless, Mg could be related to some interstratified smectite layers in illite not detected by XRD due to the low illite contents. Among major elements, the only significant correlation is that shown by Ti and Al ( $r = 0.89$ ;  $r = 0.95$  taking into account the limestone and the calcite sample too) (Fig. 3b), thus constituting an immobile element pair and indicating that Al- and Ti-bearing minerals concentrate in the same type of rock. Considering only the pisolitic samples, a negative correlation ( $r = -0.75$ ) is shown by Al and Si, as usual in bauxites.

Major element concentrations (Table 2) reveal that the clay samples are chemically more heterogeneous than the pisolitic

bauxites. When normalized to the Upper Continental Crust (UCC) concentrations (Fig. 4a), there is an enrichment in Al and Ti in both the clays and the pisolitic samples. The red pisolitic and the clay samples are also enriched in Fe, but an evident Fe depletion can be observed in the white pisolitic samples. As can be seen in Fig. 4a, both the pisolitic and the clay samples are depleted in Si, Mn, Mg, Ca, Na, K, and P although, in general, the clay samples are less depleted in Mn, Mg, Ca, K, and P. On the other hand, the change % values in Fig. 4b show that clay samples are more heterogeneous than the pisolitic ones. This figure also shows that Al, P, and to a lesser extent Si, Mn, Ca, and K are in general more depleted relative to Ti in the pisolitic samples. The pisolitic samples, particularly the white ones, tend to be Fe depleted. This is commonplace since the red colour of bauxites comes from ferric iron and therefore the white bauxite samples are indicating at least transient reducing condition invariably leading to mobilization and removal of iron (Bardossy, 1982). CIA values (Table 2) are high (>96), with those from the clay samples more heterogeneous and lower (mean value = 98.54) than those from the pisolitic bauxite (mean value = 99.83).

Fig. 5a shows some important trace element concentrations normalized to the UCC. Transition element (Sc, V, Cr, Co, Ni) normalized concentrations show an irregular trend. The only remarkable features are the relatively higher enrichment in Cr and an evident Co depletion in the pisolitic with respect to the clay samples. Also noticeable is the clearly lower V enrichment in the white pisolitic samples. With regard to the critical elements Ga and Ge, only the white pisolitic samples are slightly depleted in Ge. The

HFSE (Zr, Nb, Hf, Th, U) are always more abundant in the pisolitic samples than in the clays. Finally, the LILE (Sr, Cs, Ba) are depleted in all the samples, clearly showing that they were all subject to rather intense leaching. The average Ba/Sr ratio is higher in the clays (0.4) than in the red (0.2) and white (0.1) pisolitic samples. With regard to change % values (Fig. 5b), the transition elements are always depleted in the pisolitic bauxites. The clays are enriched in Sc and V and only slightly depleted in Cr and Ni. Ga and Ge are also depleted in bauxites and to a lesser extent in clays. The HFSE, and especially the LILE, are depleted in both the bauxites and the clays and show similar patterns regardless of the sample type. In general, as for major elements, the change % values in the clays are more heterogeneous than those of the pisolitic samples.

Y has been considered along with the REE since there is a high positive correlation between them ( $r = 0.91$ ), indicating similar behaviour. The average REE and Y contents (Table 2) of the clay samples are distinctly higher than those of the pisolitic samples, but they are much lower in the host limestone and the calcite sample. The REE + Y concentrations normalized to the UCC average (Fig. 6a) also show clear differences among the different types of samples considered. In general, the clay samples are clearly enriched in REE + Y, whereas the pisolitic samples are depleted in LREE and enriched in HREE. The limestone and the calcite cement sample are in general depleted in the REE. The highest enrichment in REE + Y in Fig. 6a corresponds to the clay sample with the highest illite contents. The REE + Y change % graph (Fig. 6b) also reveals differences: the clay samples are less depleted than the bauxites and are specifically enriched in Y and La and slightly enriched in

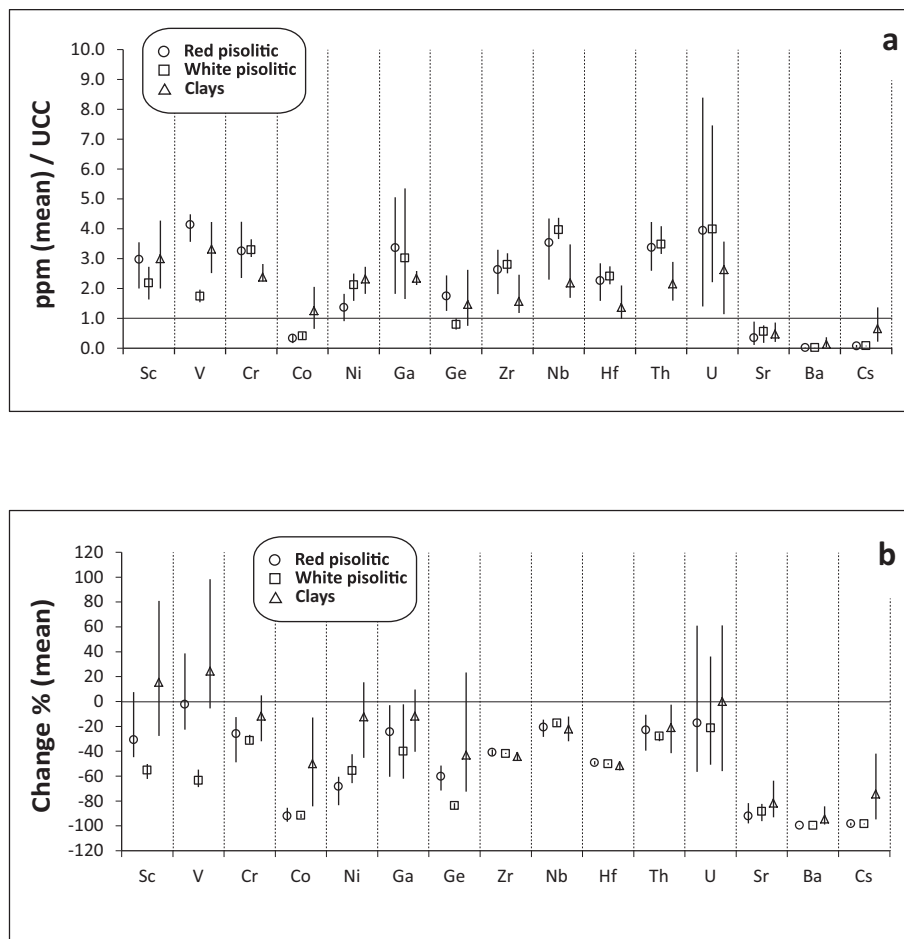
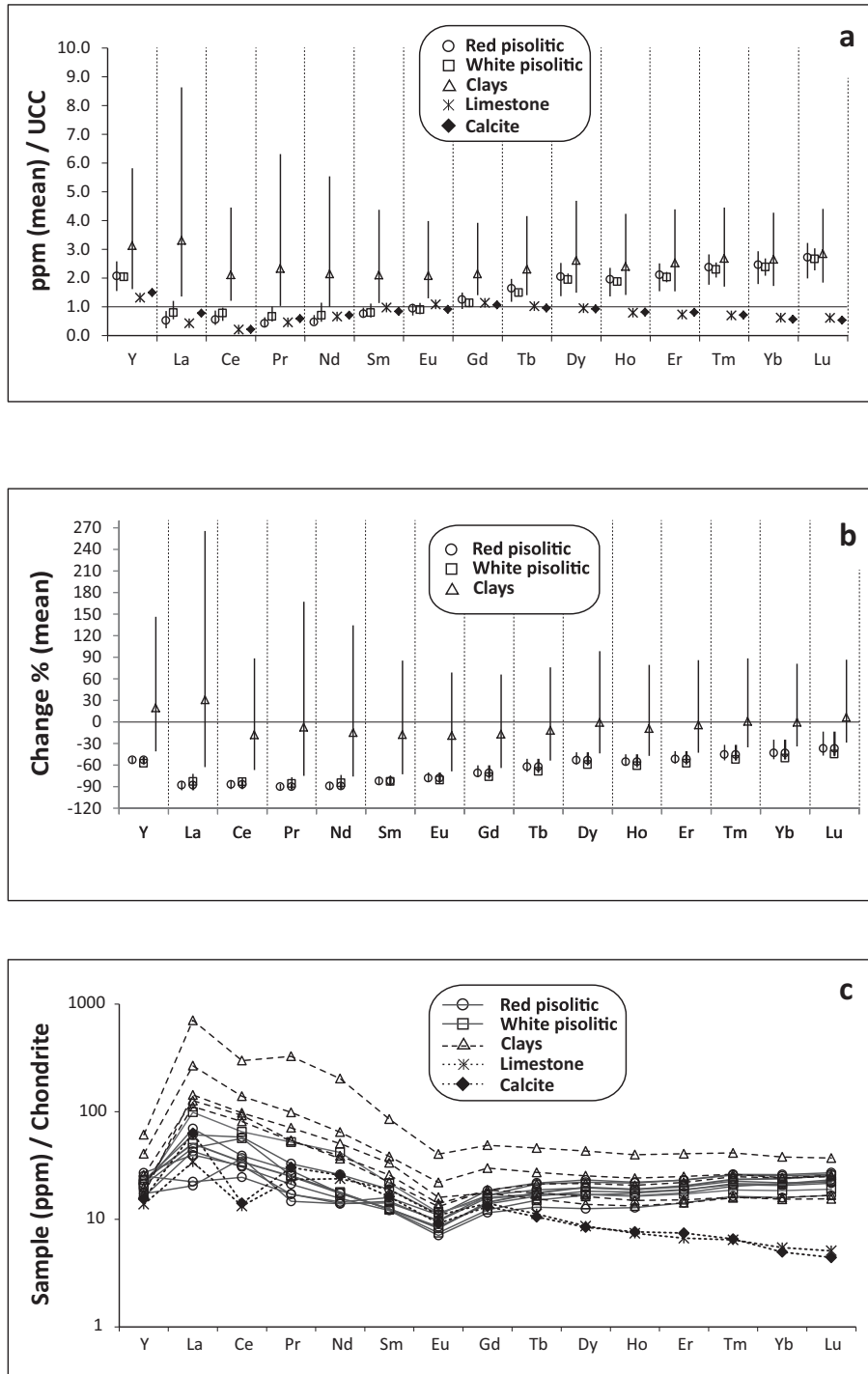


Fig. 5. a: Average and range values of some important trace elements normalized to the UCC. b: Average and range change % values of trace elements.



**Fig. 6.** a: Average and range REE + Y concentrations normalized to the UCC. b: Average and range change % values of the REE + Y. c: Chondrite-normalized REE + Y patterns of the study samples.

Lu. The highest enrichment is seen in the clay sample with high illite contents and, especially, in the host limestone and the calcite sample (not in the graph). The chondrite-normalized REE patterns (Fig. 6c) are also different depending on the group of samples considered. In both the pisolitic and the clay samples, LREE fractionation is higher than HREE fractionation, but the HREE in the clay samples show an almost horizontal slope, whereas in the pisolitic samples they show a slight upward trend. The most significant difference between the clay and the pisolitic samples (in addition to the higher REE contents in the clay samples mentioned above) is

the positive Ce anomaly observed in several pisolitic samples (especially red ones). The host limestone and the calcite cement sample REE patterns are very similar to each other, with LREE and HREE fractionation (the latter higher than that shown by the clay and the pisolitic samples) and a distinct negative Ce anomaly. All the samples show similar Eu anomaly values (Table 1). Plots of (Gd/Yb)<sub>c</sub> versus (La/Sm)<sub>c</sub> and Ce/Ce\* versus (La/Yb)<sub>c</sub> in Fig. 7 (values in Table 2) allow the three groups of samples to be distinguished. Fig. 7a shows higher LREE and HREE fractionation in the clay samples compared to the pisolitic ones. On the other hand,



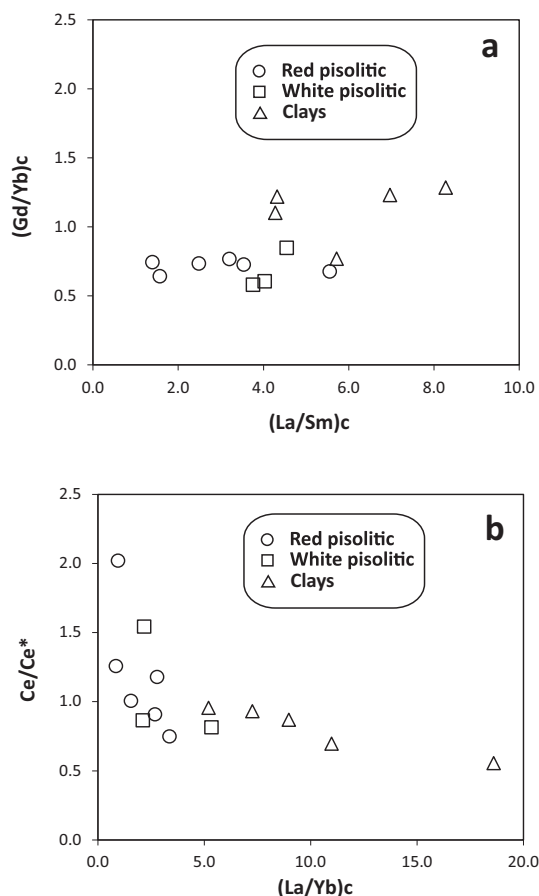


Fig. 7. Plots of a:  $(La/Sm)_c$  vs.  $(Gd/Yb)_c$ , and b:  $(La/Yb)_c$  vs.  $Ce/Ce^*$ .

Fig. 7b shows lower REE fractionation of the pisolitic samples and higher Ce anomalies of these samples, followed by the clay samples.

## 5. Discussion

Several studies on karst bauxite deposits have proposed that bauxite formed from lateritized material precursor (Valeton, 1972; Ling et al., 2015), ferruginous-argillaceous debris (Zarasvandi et al., 2008), or clayey (mainly kaolinitic) material (MacLean et al., 1997; Oggiano and Mameli, 2001). A previous study of the Fuentespalda karst bauxite deposit proposed that pisolitic bauxite originated *in situ* from precursor lateritic clays through a complex sequence of mineralogical processes (Yuste et al., 2015). According to these authors, the bauxitization process occurred from the top down, preventing the lower part of the profile from being entirely bauxitized and resulting in preservation of the lateritic parent clays underlying the pisolitic bauxite. Karst reactivation subsequent to bauxitization caused the present heterogeneous-chaotic lithostructure of the deposits, following the classic scheme by Combes (1969).

The high correlation ( $r = 0.94$ ) between Ti and Al (Fig. 3a) is related to the formation of Al-rich minerals and to Ti oxides, indicating an immobile nature for these major elements in the bauxitization process, as traditionally considered (Nesbitt, 1979; Sastri and Sastry, 1982; Valeton et al., 1987; MacLean, 1990; Gow and Lozej, 1993). The trend from clay to pisolitic samples shown in that figure also supports the idea that the clay materials closely associated to the pisolitic bauxite are their precursors. The more hetero-

geneous chemical character of the clay samples also points in this direction and probably reflects a greater detrital influence related to less and variable weathering compared to the pisolitic samples. This is also supported by the more variable and less crystalline nature of kaolinite from the clay samples, as Yuste et al. (2015) reported. CIA values, higher than those of the UCC (60.11), are more heterogeneous and lower in the clay samples compared to the pisolitic ones, which is in agreement with the above ideas. Regarding the change % data, the widespread higher depletion recorded by the pisolitic bauxite relative to the clays has to be interpreted as a result of more intense weathering that led to the formation of bauxite from the precursor. The mineralogical characteristics of the clay samples and their chemical classification as laterites support the notion that these materials are precursor aluminous clays for the pisolitic bauxite, and are probably related to the lateritic clays from the Cantaperdius Fm. described by Salas (1987) and Molina and Salas (1993). The scenario first included the formation of the clays through ferrallitization and edaphic processes favoured by periodic subaerial exposure in a tropical climate (Molina and Salas, 1993). Palaeogeographic conditions and ongoing weathering permitted bauxitization of this precursor. Subsequently, late kaolinization processes (resilicification) took place (Yuste et al., 2015). The higher Al depletion in the pisolitic samples (Fig. 4b) could be related to these processes subsequent to bauxitization involving partial replacement of gibbsite by kaolinite in the pisolitic bauxite, as Yuste et al. (2015) pointed out. According to these authors, this replacement was more pronounced in the white pisolitic bauxite, which is supported by the slightly higher Si depletion in the red pisolitic samples. Nevertheless, these late processes did not lead to an absolute Si enrichment in the pisolitic samples, as revealed by the change % values. In West Sardinian karst bauxite, for example,  $SiO_2$  addition has been well documented and related to low-temperature solutions linked to Oligocene-Miocene calc-alkaline volcanic activity (Oggiano et al., 1987; Oggiano and Mameli, 2001). In the present case, no post-Jurassic magmatism has been documented, and therefore we must turn to solutions acid enough to induce Al hydroxide dissolution and a decrease in  $SiO_2$  solubility favouring kaolinite recrystallization. The palaeokarst where the bauxites are hosted was fossilized by Albian formations which in the Maestrazgo Basin include materials rich in organic matter and coal. These materials could have played a significant role in the acidification of fluids responsible for karst reactivation and related bauxite kaolinization.

In general, based on Fe change % values, the more intense weathering related to the bauxitization process led to Fe loss and probably to its accumulation in the underlying clays. Not surprisingly, then, the precursor clays are clearly enriched in this element compared to the pisolitic bauxites. This Fe loss was aggravated by more pronounced late kaolinization processes in the white pisolitic bauxite, as indicated by the higher Fe depletion in these samples. Fe concentrations normalized to the UCC also support this.

Taking into account concentrations normalized to the UCC, bauxites are relatively more enriched in Cr, Ga, Zr, Nb, Hf, Th, and U and depleted in Co (and in Ge in the case of the white pisolitic samples). The only ones of these elements that show a good positive correlation with each other and with Ti and Al are Zr and Cr (Fig. 8), and thus they can be considered as immobile elements during bauxitization. Nevertheless, in absolute terms, bauxitization has promoted higher trace element depletion (except for Zr, Nb, and Hf, which show similar values in both bauxites and clays) than lateritic processes, which is related to the more intense weathering (as deduced from the change % values). This is also supported by the observed Ba/Sr average ratios, since Sr is much more soluble than Ba (Retallack, 1990). The low Cr depletion observed in Fig. 5b and the similar values shown by both bauxites and clays support the idea of its less mobile nature along with Zr and prob-

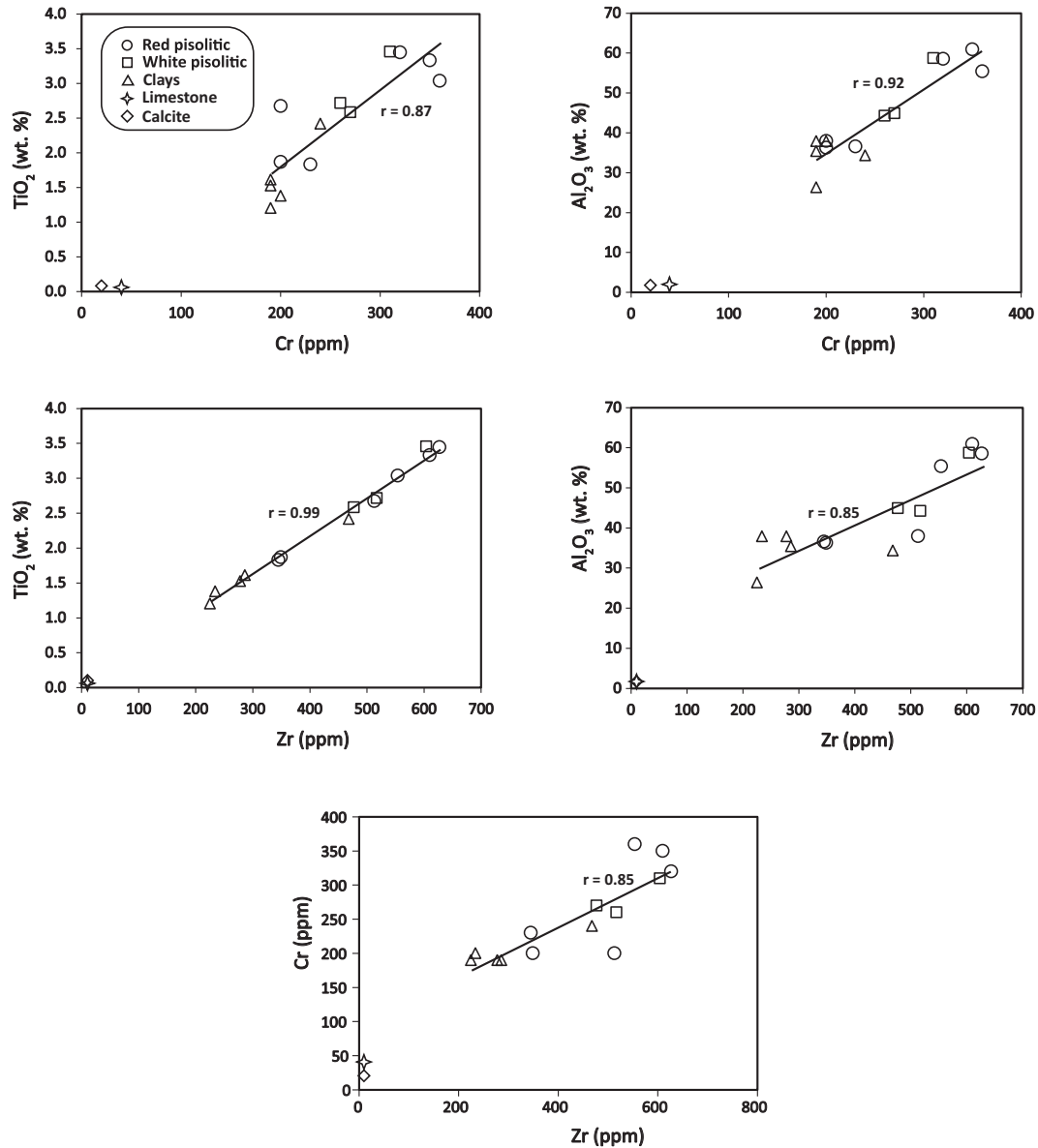


Fig. 8. Plots of Cr and Zr vs.  $\text{TiO}_2$  and  $\text{Al}_2\text{O}_3$  and Zr vs. Cr.

ably Nb and Hf. In addition, bauxitization has led to chemical homogenization taking into account the more heterogeneous values shown by the clay samples. On the other hand, it is worth mentioning the slight enrichment in Sc and V recorded in the lateritic clays that would be derived from the lateritic process. The evident V and, to a lesser extent, Sc and Ge depletion observed in the white samples seems to be linked to the late kaolinization process as it shows a trend similar to Fe.

Most of the REE in karst bauxites are bound to detrital minerals inherited from the source rock but they also fractionate during the bauxitization process (Maksimovic and Roaldset, 1976; Maksimovic and Pantó, 1991), and can be adsorbed on the surface of clay minerals (see Wang et al., 2010, and references therein) or Fe phases (Mongelli, 1997; Mameli et al., 2007). In addition, as Maksimovic and Pantó (1978, 1991) have shown, fractionation can take place through the formation of authigenic REE minerals.

The higher REE + Y contents in the clay samples could be related to a variety of inherited minerals in agreement with their more detrital nature, supported by the more ubiquitous presence of illite in these samples. In fact, the sample with the highest REE + Y con-

tents is that with the highest illite contents. In addition, the higher REE + Y content in the clay samples would have been enhanced by the downward enrichment of REE in the lowermost part of karst bauxites during the bauxitization process, as D'Argenio and Mindszenty (1995, and references therein) indicated, and Maksimovic and Pantó (1991) showed in the karst bauxite deposits of Yugoslavia and Greece. The transformation of the clays into pisolitic bauxite therefore involved REE + Y loss. High positive correlations have been found between REE and Cs ( $r = 0.94$ ) and Co ( $r = 0.87$ ), indicating similar behaviour of these elements during bauxitization. REE + Y change % values (Fig. 6b) support the above idea since pisolitic samples show a clear depletion in these elements, especially the LREE. From this graph, it can be also deduced that bauxitization tends to homogenize REE + Y concentrations, as observed in trace elements, since clays show more heterogeneous values. This trend is also shown by the REE + Y concentrations normalized to the UCC (Fig. 6a). That is to say, the more intense the chemical weathering (i.e. bauxitization vs ferrallitization), the more LREE depletion can be expected, in agreement with Maksimovic and Pantó (1991).

The lower (La/Sm)<sub>c</sub>, (La/Yb)<sub>c</sub>, and (Gd/Yb)<sub>c</sub> average values (lower fractionation) in the pisolitic samples are most likely linked to the concentration of certain immobile phases that act as scavengers for the REE as weathering progresses. In addition, the higher LREE over HREE fractionation indicates that the HREE were less mobile than the LREE. This could be attributed to the concentration of heavy minerals like rutile and anatase, which might have acted as scavengers for HREE, as occurred in the south Turkish bauxite deposits reported by Karadag et al., 2009. On the other hand, some authors (Nyakairu et al., 2001; Kanazawa and Kamitani, 2006; Roy and Smykatz-Kloss, 2007) have reported on the importance of P-bearing phases as LREE carriers. In this regard, SEM observations of the study samples have evidenced a more frequent occurrence of xenotime, apatite, and Al phosphate-sulfate (APS) minerals in the clay samples (Fig. 9), whereas Ti oxides are more common in the pisolitic ones, in agreement with chemical data (Fig. 4). These observations would explain the reported LREE and HREE trends in the pisolitic samples compared to the clay ones. The positive correlation between the LREE and P<sub>2</sub>O<sub>5</sub> ( $r = 0.60$ ) would support the above ideas, but the poor negative correlation found between the HREE and TiO<sub>2</sub> ( $r = -0.21$ ) indicates that minerals other than Ti oxides are related to the REE behaviour during bauxitization. As Bardossy and Panto (1973), Maksimovic and Pantó (1991), Mongelli (1997), and Marnelli et al. (2007) have indicated, fluorocarbonate minerals of the bastnäsité group are the most frequent REE minerals in Mediterranean karst bauxite deposits, although these minerals have not yet been identified in the Fuentespalda deposit.

With regard to the cited frequent positive Ce anomaly in the pisolitic samples, several researchers (Braun et al., 1990; Nyakairu et al., 2001; Compton et al., 2003) have reported that Ce is usually retained in the upper parts of the weathering profiles due to the oxidation of Ce(III) to the less mobile Ce(IV). This supports the idea of in-situ bauxitization occurring from the top down suggested by Yuste et al. (2015). The negative Ce anomaly recorded

in some pisolitic samples would be related to variable oxidation conditions favouring Ce(III) over Ce(IV), probably related to the afore-mentioned acidic and reducing solutions, which promoted late kaolinization stages. In fact, white pisolitic samples show a lower average Ce anomaly value.

Bardossy and Aleva (1990) stated that the textures and composition of most lateritic bauxites can be used to relate them directly to the underlying source rocks, but this is not the case in karst bauxites. In the present study, the pisolitic bauxite is derived from the clays with which they are closely associated in the karst cavities they fill. As Mongelli (1993) (among others) has indicated, the Eu anomaly has proven to be retained during intense weathering and the fact that the observed Eu anomaly values in both the pisolitic and the clay samples are very similar supports their genetic relationship. In addition, as pointed out above, Al, Ti, and Cr have behaved as immobile elements during bauxitization and therefore the TiO<sub>2</sub>/Al<sub>2</sub>O<sub>3</sub> and Ti/Cr ratios can be considered as sensitive indices of parental affinity. Plots of these ratios against Eu anomaly values have been used in other Mediterranean karst bauxites to decipher the parental affinity of the bauxites, that is, the bauxite deposits from Nurra (Italy) studied by Marnelli et al. (2007). As can be observed in Fig. 10a, Eu/Eu\* is similar to the UCC, but TiO<sub>2</sub>/Al<sub>2</sub>O<sub>3</sub> departs from the UCC and tends towards more mafic compositions. This may be due in part to the Al depletion relative to Ti deduced from the change % values, as commented above. Similarly, Ti/Cr values also depart from the UCC with an average value half-way between the UCC and the average basalt composition (Fig. 10b). This points to an intermediate source with a parental affinity slightly more mafic than the UCC for the argillaceous sediments from which first aluminous clays, and subsequently bauxite developed through intense chemical weathering.

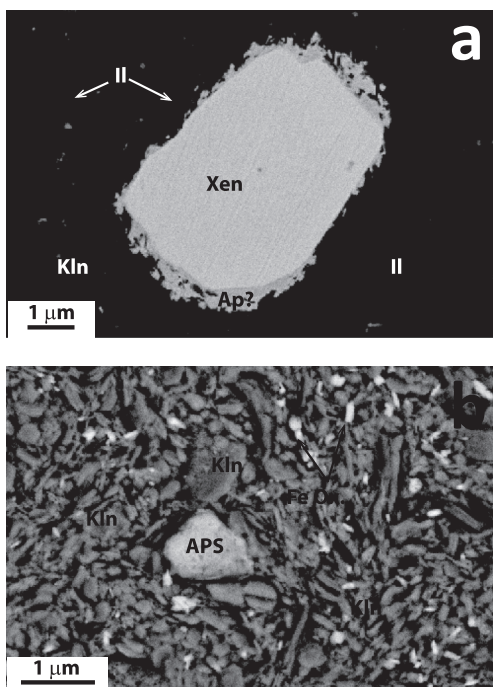


Fig. 9. Backscattered electron (BSE) images of clay samples. a: Y-rich mineral (xenotime) showing an irregular growth rim of probable apatite (Ap). b: Al phosphate-sulphate (APS) mineral. Xen: xenotime; Ill: illite; Kln: kaolinite; Fe Ox.: iron oxides.

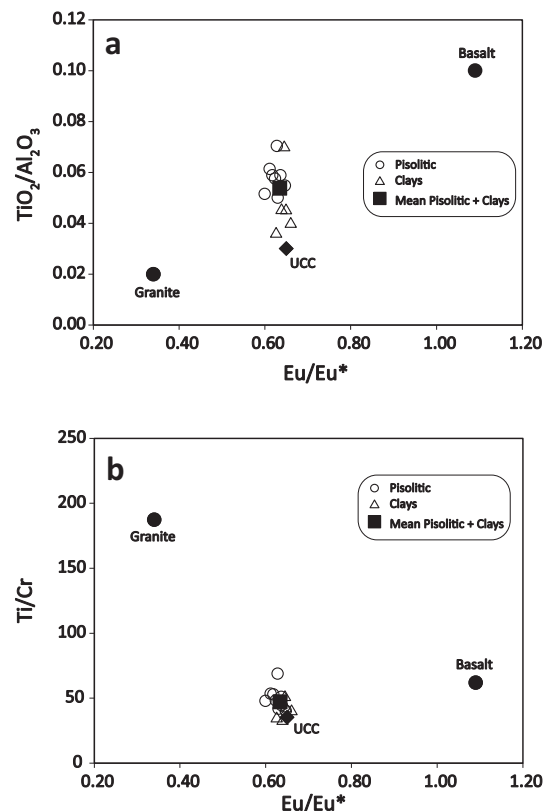


Fig. 10. Plots of Eu/Eu\* vs. TiO<sub>2</sub>/Al<sub>2</sub>O<sub>3</sub> (a) and Ti/Cr (b). Granite and basalt compositions are from Condie (1993).

## 6. Conclusions

This research indicates that the studied karst bauxites are derived from the Al-rich clays with which they are closely related. Bauxitization of the clays was the result of intense weathering taking place from the top down. This prevented the lower parts of the weathering profile from being bauxitized and resulted in the aluminous clays underlying the pisolitic bauxite. Consequently, the clays geochemistry reflects variable weathering and a greater detrital influence. Compared to ferrallitization, bauxitization led to chemical homogenization and widespread higher element depletion. During the process, Al and Ti behaved as an immobile element pair, whereas Fe was variably leached. Nevertheless, processes subsequent to bauxitization caused some Al depletion in the bauxite, related to the partial replacement of gibbsite by kaolinite. This replacement, which increased the loss of Fe, was favoured by the circulation of acid solutions that triggered karst reactivation, which gave rise to the present heterogeneous-chaotic lithostructure of the deposits.

UCC-normalized trace-element concentrations have revealed that bauxites are enriched in some elements compared to clays, including the critical element Ga. Nevertheless, in absolute terms, ferrallitization can be linked to Sc and V enrichment, whereas bauxitization has promoted chemical depletion, except for Zr, Cr, and probably the critical elements Nb and Hf, which can be considered immobile during the process. On the other hand, V and, to a lesser extent, Ge show behaviour similar to Fe, and therefore they were depleted during the late kaolinization process.

The higher degree of weathering related to bauxitization also involved the homogenization of REE + Y concentrations and their depletion during the transformation of ferrallitized clays into bauxites. This depletion is more pronounced for the LREE. The mobility and fractionation behaviour of the REE is linked to the concentration of minerals that act as scavengers for these elements. Ti oxides preferably scavenge the HREE, but other minerals, like fluorocarbonates of the bastnäsite group, cannot be ruled out. Further research needs to be carried out on this point since no fluorocarbonates have been detected yet in the studied karst bauxites. On the other hand, the LREE seem to show a preference for P-bearing phases, more frequent in the clay precursor of the bauxites.

Intense chemical weathering, responsible for the development of the aluminous clays first and subsequently the bauxites, did not modify the Eu anomaly. This anomaly, together with the Ti, Al, and Cr ratios, suggests an intermediate character slightly more mafic than the UCC for the argillaceous sediments from which the Al-rich clays and bauxites originated.

## Acknowledgements

This research has been funded by the Spanish Ministerio de Economía y Competitividad (CGL2013-46169-C2-1-P) and the Gobierno de Aragón and the European Social Fund (Grupo Consolidado, Recursos Minerales E45). We are grateful to the journal reviewers for their helpful comments and to Ore Geology Reviews Editors for revision and editorial handling of the manuscript. The authors also acknowledge the use of the Servicio de Apoyo a la Investigación-SAI, University of Zaragoza (Spain), and Christine Laurin for revising the English text.

## References

Aleva, G.J.J., 1994. Laterites: Concepts, Geology, Morphology and Chemistry. International Soil Reference and Information Centre (ISRIC), Wageningen, The Netherlands.

Bardossy, G., 1982. Karst Bauxites. Bauxite Deposits on Carbonate Rocks. Elsevier, Amsterdam.

Bardossy, G., Aleva, G.J.J., 1990. Lateritic bauxites. In: Developments in Economic Geology, vol. 27. Elsevier, Amsterdam.

Bardossy, G., Panto, G., 1973. Trace mineral and element investigation in bauxites by electron probe. In: ICSOBA 3rd Int. Congr. Nice, pp. 47–53.

Braun, J.J., Pagel, M., Muller, J.P., Bilong, P., Michard, A., Guillet, B., 1990. Ce anomalies in lateritic profiles. *Geochim. Cosmochim. Acta* 54, 781–795.

Combes, P.J., 1969. Recherches sur la genèse des bauxites dans le Nord-Est de l'Espagne, Le Languedoc et l'Ariège (France) (Ph.D Thesis). Université de Montpellier.

Compton, S.J., White, A.R., Smith, M., 2003. Rare earth element behavior in soils and salt pan sediments of a semi-arid granitic terrain in the Western Cape, South Africa. *Chem. Geol.* 201, 239–255.

Condie, K.C., 1993. Chemical composition and evolution of the upper continental crust: contrasting results from surface samples and shales. *Chem. Geol.* 104, 1–37.

Cullers, R.L., Graf, J., 1983. Rare earth elements in igneous rocks of the continental crust: intermediate and silicic rocks, ore petrogenesis. In: Henderson, P. (Ed.), *Rare Earth Element Geochemistry*. Elsevier, Amsterdam, pp. 275–312.

D'Argenio, D., Mindszenty, A., 1995. Bauxites and related paleokarst: tectonic and climatic event markers at regional unconformities. *Eclogae Geol. Helv.* 88 (3), 453–499.

Gow, N.N., Lozej, G.P., 1993. Bauxite. *Geosci. Can.* 20, 9–16.

Guimerà, J., Mas, R., Alonso, A., 2004. Intracratonic deformation: from Mesozoic extension to Tertiary contractional inversion in the northwest Iberian Chain. *J. Geol. Soc.* 161, 291–303.

Kanazawa, Y., Kamitani, M., 2006. Rare earth minerals in the world. *J. Alloy Compd.* 408–412, 1339–1343.

Karadag, M.M., Küpeli, S., Aryk, F., Ayhan, A., Zedef, V., Döyen, A., 2009. *Chem. Erde Geochem.* 69, 143–159.

Ling, K., Zhu, X., Tang, H., Wang, Z., Yan, H., Han, T., Chen, W., 2015. Mineralogical characteristics of the karstic bauxite deposits in the Xiufen ore belt, Central Guizhou Province, Southwest China. *Ore Geol. Rev.* 65, 84–96.

Liu, X., Wang, Q., Feng, Y., Li, Z., Cai, S., 2013. Genesis of the Guangou karstic bauxite deposit in western Henan. *Ore Geol. Rev.* 55, 162–175.

MacLean, W.H., 1990. Mass change calculations in altered rock series. *Miner. Deposita* 25, 44–49.

MacLean, W.H., Bonavia, F.F., Sanna, G., 1997. Argillite debris converted to bauxite during karst weathering: evidence from immobile element geochemistry at the Olmedo Deposit, Sardinia. *Miner. Deposita* 32, 607–616.

Maksimovic, Z., Pantó, G., 1978. Minerals of the rare-earth elements in karstic bauxites: synchysite-(Nd), a new mineral from Grebnik deposit. In: IV Int. Congr. ICSOBA, Athens, vol. 1, pp. 540–552.

Maksimovic, Z., Pantó, G., 1991. Contribution to the geochemistry of the rare earth elements in the karst-bauxite deposits of Yugoslavia and Greece. *Geoderma* 51, 93–109.

Maksimovic, Z., Roaldset, E., 1976. Lanthanide elements in some Mediterranean karstic bauxite deposits. *Travaux ICSOBA* 13, 199–220.

Mameli, P., Mongelli, G., Oggiano, G., Dinelli, E., 2007. Geological, geochemical and mineralogical features of some bauxite deposits from Nurra (Western Sardinia, Italy): insights on conditions of formation and parental affinity. *Int. J. Earth Sci. (Geol. Rundsch.)* 96, 887–902.

Mas, R., Salas, R., 2002. Lower Cretaceous of the Iberian Basin. In: Gibbons, W., Moreno, T. (Eds.), *The Geology of Spain*. Geol. Soc., London, pp. 284–288.

Mas, R., Guimerà, J., Alonso, A., 1998. The Cameros Basin (North Spain): a typical intraplate extensional basin in the Mesozoic Iberian Rift System. In: *Sedimentology at the dawn of the third millennium*. Sedim. Congr., Alicante, pp. 539–540.

Mas, R., García, A., Salas, R., Meléndez, A., Alonso, A., Aurell, M., Bádenas, B., Benito, M.I., Carenas, B., García-Hidalgo, J.F., Gil, J., Segura, M., 2004. Segunda Fase de rifting: Jurásico Superior-Cretácico Inferior. In: Vera, J.A. (Ed.), *Geología de España*. SGE-IGME, Madrid, pp. 503–510.

Molina, J.M., Salas, R., 1993. Bauxitas kársticas del Cretácico inferior en Fuentespalda (provincia de Teruel): Estratigrafía, origen y paleogeografía. *Cuad. de Geol. Ibérica* 17, 207–230.

Mongelli, G., 1993. REE and other trace elements in a granitic weathering profile from "Serre", Southern Italy. *Chem. Geol.* 103, 17–25.

Mongelli, G., 1997. Ce-anomalies in the textural components of Upper Cretaceous karst bauxites from the Apulian carbonate platform (Southern Italy). *Chem. Geol.* 140, 69–79.

Mongelli, G., Boni, M., Buccione, R., Sinisi, R., 2014. Geochemistry of the Apulian karst bauxites (southern Italy): chemical fractionation and parental affinities. *Ore Geol. Rev.* 63, 9–21.

Mongelli, G., Buccione, R., Gueguen, E., Langone, A., Sinisi, R., 2016. Geochemistry of the apulian allochthonous karst bauxite, Southern Italy: distribution of critical elements and constraints on Late Cretaceous Peri-Tethyan palaeogeography. *Ore Geol. Rev.* 77, 246–259.

Nesbitt, H.W., 1979. Mobility and fractionation of rare earth elements during weathering of a granodiorite. *Nature* 279, 206–279.

Nesbitt, H.W., Young, G.M., 1982. Early proterozoic climates and past plate motions inferred from major element chemistry of lutites. *Nature* 299, 715–717.

Nyakairu, G.W.A., Koerber, C., 2001. Mineralogical and chemical composition and distribution of rare earth elements in clay-rich sediments from Central Uganda. *Geochem. J.* 35, 13–28.

Nyakairu, G.W.A., Koerber, C., Kurzweil, H., 2001. The Buwambo kaolin deposit in Central Uganda: mineralogical and chemical composition. *Geochem. J.* 35, 245–256.

- Oggiano, G., Mameli, P., 2001. The bauxite of North-Western Sardinia. *Rendiconti della Facoltà di Scienze MM.FF.NN. dell'Università di Cagliari* 71 (II), 59–73.
- Oggiano, G., Sanna, G., Temussi, I., 1987. Caractères géologiques, géologiques et géochimiques de la bauxite de la Nurra. In: Chechi, A. (Ed.), *Livret-Guide Excursion En Sardaigne 24–29 Mai 1987*, Chechi, A. Groupe Français du Crétacé, Cagliari, pp. 72–124.
- Retallack, G.J., 1990. *Soils of the Past: An Introduction to Paleopedology*. Unwin-Hyman, London.
- Roy, P.D., Smykatz-Kloss, W., 2007. REE geochemistry of the recent playa sediments from the Thar Desert, India: an implication to playa sediment provenance. *Chem. Erde Geochem.* 67, 55–68.
- Salas, R., 1987. El Malm y el Cretaci inferior entre el Massis de Garraf i la Serra d'Espadà (Ph.D Thesis). University of Barcelona.
- Salas, R., Casas, A., 1993. Mesozoic extensional tectonics, stratigraphy and crustal evolution during the Alpine cycle of the eastern Iberian basin. *Tectonophysics* 228, 33–55.
- Salas, R., Guimerà, J., Mas, R., Martín-Closas, C., Meléndez, A., Alonso, A., 2001. Evolution of the Mesozoic Central Iberian Rift System and its Cainozoic inversion (Iberian Chain). In: Cavazza, W., Roberston, A.H.F.R., Ziegler, P., Crasquin-Soleau, S. (Eds.), *Peri-Tethyan Rift/Wrench Basins and Passive Margins*. *Mém. Mus. Nat. Hist. Natur.*, vol. 186, pp. 145–185.
- Sastri, G.G.K., Sastry, C.S., 1982. Chemical characteristics and evolution of the laterite profile in Hazaridadar Bauxite Plateau, Madhya Pradesh, India. *Econ. Geol.* 77, 154–161.
- Schellmann, W., 1986. On the geochemistry of laterites. *Chem. Erde Geochem.* 45, 39–42.
- Tardy, Y., 1986. Le cycle de l'eau. *Climats, paléoclimats et géochimie globale*. Masson, Paris.
- Taylor, S.R., McLennan, S.M., 1985. *The Continental Crust: Its Composition and Evolution*. Blackwell, Oxford.
- Taylor, S.R., McLennan, S.M., 1995. The geochemical evolution of the continental crust. *Rev. Geophys.* 33, 241–265.
- Valeton, I., 1972. Bauxites. *Developments in Soil Science*, vol. 1. Elsevier, Netherlands.
- Valeton, I., Biermann, M., Reche, R., Rosenberg, F., 1987. Genesis of nickel laterites and bauxites in Greece during the Jurassic and Cretaceous, and their relation to ultrabasic parent rocks. *Ore Geol. Rev.* 2, 359–404.
- Van Wees, J.D., Arche, A., Bejedorff, C.G., López-Gómez, J., 1998. Temporal and spatial variations in tectonic subsidence in the Iberian Basin (eastern Spain): inferences from automated forward modelling of high-resolution stratigraphy (Permian-Mesozoic). *Tectonophysics* 300, 285–310.
- Wang, Q., Deng, J., Liu, X., Zhang, Q., Sun, S., Jiang, C., Zhou, F., 2010. Discovery of the REE minerals and its geological significance in the Quyang bauxite deposit, West Guangxi, China. *J. Asian Earth Sci.* 39, 701–712.
- Yuste, A., Bauluz, B., Mayayo, M.J., 2015. Genesis and mineral transformations in Lower Cretaceous karst bauxites (NE Spain): climatic influence and superimposed processes. *Geol. J.* 50, 839–857.
- Zarasvandi, A., Charchi, A., Carranza, E.J.M., Alizadeh, B., 2008. Kars bauxite deposits in the Zagros Mountain Belt, Iran. *Ore Geol. Rev.* 34, 521–532.